Temperature-Sensitive Hydrogel-Particle Films from Evaporating Drops

Tim Still, Peter J. Yunker, Kasey Hanson, Zoey S. Davidson, Matthew A. Lohr, Kevin B. Aptowicz, and A. G. Yodh*

A simple method to prepare temperature-sensitive films composed of micrometer-sized colloidal hydrogel particles using evaporating drops of colloidal suspensions is demonstrated. The films range in thickness from a monolayer to approximately fifty particle diameters depending on initial particle volume fraction. Sessile droplets of hydrogel-particle suspensions are evaporated on silicon wafers. The film is formed from particles spread densely over the air–water interface which then cross-link and are deposited on the surface during the evaporation process. The resultant thin films exhibit a temperature-responsiveness characteristic of the individual particles permitting modulation of size, shape, porosity, and optical transmission.

1. Introduction

Films and membranes are ubiquitous structures whose defining properties range from selective light transmission and porosity to variable strength and size/shape. Thus, creative design of films and membranes is an exciting scientific endeavor spanning both hard and soft materials, which in some cases has led to important uses, for example in permeability applications.[1–4] To this end, we demonstrate the utility of the evaporating colloidal drop as a simple means to create aqueous micron-thick colloidal particle films with controllable shape and porosity; these films possess potentially useful environmental responses, including light transmission, porosity, elastic modulus, and size/shape. The single-step film assembly method takes advantage of both the temperature sensitivity and the unique evaporation/deposition properties of poly(*N*-isopropyl acrylamide) (PNIPAM) hydrogel particles in water drops.

Drying drops of colloidal particle suspensions typically leave a thin ring-shaped stain that contains most of the solid material that was initially suspended. This highly nonuniform deposition is known as the coffee-ring effect; it is produced when the drop edges are pinned during evaporation and subsequent radial capillary flows from the drop center carry suspended solutes to the drop perimeter.[5–7] The coffee-ring effect, however, can be ameliorated in aqueous systems of large (>10 μm) suspended spheres,[8] in suspensions of ellipsoidal particles with strong capillary interactions,[9] via electrowetting,[10] in systems with strong attractive forces between particles and substrate,[11] and in the presence of surfactants that lead to strong Marangoni flows,[12,13] among other techniques.[14–16] In these cases, the drying drop system provides experimenters with an opportunity to make uniform thin particle coatings and films.

The present contribution builds on investigations of Horigome and Suzuki, which demonstrated that drying aqueous suspensions of PNIPAM particles on polystyrene substrates did not yield typical coffee-ring deposition.[17] Rather, the hydrogel particles tend to act as amphiphilic moieties, populating the air–water interface fairly uniformly during evaporation.[18] This behavior, also observed for linear PNIPAM polymers,[19,20] induces a predominantly uniform deposition of hydrogel particles on the substrate. In our work, we employ micrometer-size (diameter d = 1–4 μm) PNIPAM microgel particles with comonomer 2-aminoethylmethacrylate hydrochloride (AEMA) in the suspension. Importantly, the AEMA comonomer introduces primary amine groups onto the microgel particle surfaces that can be used for subsequent cross-linking. Much smaller (<100 nm) PNIPAM particles are feasible,[21] but systematic studies on the introduction of amine groups still have to be performed. On the other end of the spectrum, we can prepare functionalized particles with amine groups up to approximately 10 μm with the referenced methods. Even larger particles are achievable using microfluidic techniques.

After the water has evaporated, a mostly uniform microgel particle film remains on the substrate. It is kept untouched for another 24 h to ensure cross-linking of neighboring particles by glutaraldehyde that is also mixed into the original droplet suspension. The resultant hydrogel-particle film is temperature-sensitive because the hydrogel particles that compose it are temperature-sensitive. Thus, film size, shape, porosity, and even optical properties are readily varied with temperature control.

Our novel responsive films can be utilized as membranes that differ from film structures that have been previously

Dr. T. Still, K. Hanson, Z. S. Davidson, Dr. M. A. Lohr, Prof. A. G. Yodh
Department of Physics and Astronomy
University of Pennsylvania
Philadelphia, PA 19104, USA
E-mail: timstill@seas.upenn.edu
Prof. P. J. Yunker
School of Physics
Georgia Institute of Technology
Atlanta, GA 30332, USA
Prof. K. B. Aptowicz
Department of Physics
West Chester University
West Chester, PA 19383, USA

DOI: 10.1002/admi.201500371

explored. Hydrogel-polymer-based membranes, for example, have been prepared as thin polymer films with porosities in the 10 nm range,[22–24] by cross-linking polymer spheres within hydrogel background media,[25] or by crafting the insides of the pores of hydrogel-free membranes with hydrogel material.[4,26] Colloidal membranes have also been prepared by multistep template-based syntheses starting from self-assembled ordered and disordered colloidal silica particle packings.[27,28] To date, most of these approaches require a series of preparation steps or yield only small membranes that are 3D in nature. By contrast, thin films made from hydrogel spheres can be synthesized from a range of particle sizes (e.g., with dimensions ranging from tens of nanometers to micrometers). Therefore, membrane properties such as responsiveness, porosity, and light transmission/scattering can be controlled. In this contribution, we describe the synthesis of such membrane structures and associated mechanisms, and we demonstrate and model some temperature-dependent properties of the resulting films.

2. Results and Discussion

The colloids used for these studies are composed of micrometer-size PNIPAM hydrogel particles (d = 1–4 μm) in water, synthesized following published procedures.[29,30] Specifically, we employ a semi-batch synthesis scheme in the presence of AEMA comonomer presented in section 2(a,b) of ref. [29] and the one-pot synthesis described in ref. [30], respectively. The AEMA comonomer enables synthesis of larger particle sizes, and it also introduces primary amine groups onto the particle surfaces that can be used for subsequent cross–linking. We then prepare aqueous suspensions of these PNIPAM particles with volume fractions of $\phi \approx$ 20%–30% (at room temperature) and 2–3 vol% glutaraldehyde cross-linker. (Note that for hydrogel particles volume fraction is defined as the total volume of the swollen hydrogel spheres divided by the total volume of the suspension.)

Sessile drops with diameters ranging from ≈0.5–3.5 cm containing 100–300 μL of this suspension are placed on a polished silicon wafer, where they evaporate under ambient lab conditions (≈22 °C, ≈50% rel. humidity) for approximately two hours. After the water has evaporated, the mostly uniform particle film remaining on the substrate is kept untouched for another 24 h in order to facilitate complete cross-linking of the amine groups of neighboring particles with glutaraldehyde. The resulting cross-linked films are then easily removed from the silicon substrate by submerging the wafer in a water bath until the film detaches from the wafer (24–48 h).

The deposition of PNIPAM colloidal particles on the silicon substrates was found to be in rough agreement with observations of drying PNIPAM suspensions on polystyrene substrates.[17] **Figure 1**a–d shows photographic images of a drying drop that produces a thin colloidal film. The three-phase contact line is pinned for the majority of the evaporation time (Figure 1a,b), with some depinning starting only after more than 1 h (Figure 1c). This behavior is consistent with particle-induced self-pinning that has been observed in numerous drying drops.[17,31] The final deposition after about 130 min (Figure 1d) is a film that consists primarily of a thin layer of densely packed PNIPAM particles cross-linked with glutaraldehyde. Depending on the initial particle concentration ϕ, the film thickness can range from a monolayer (at low $\phi \approx$ 1%)[17]

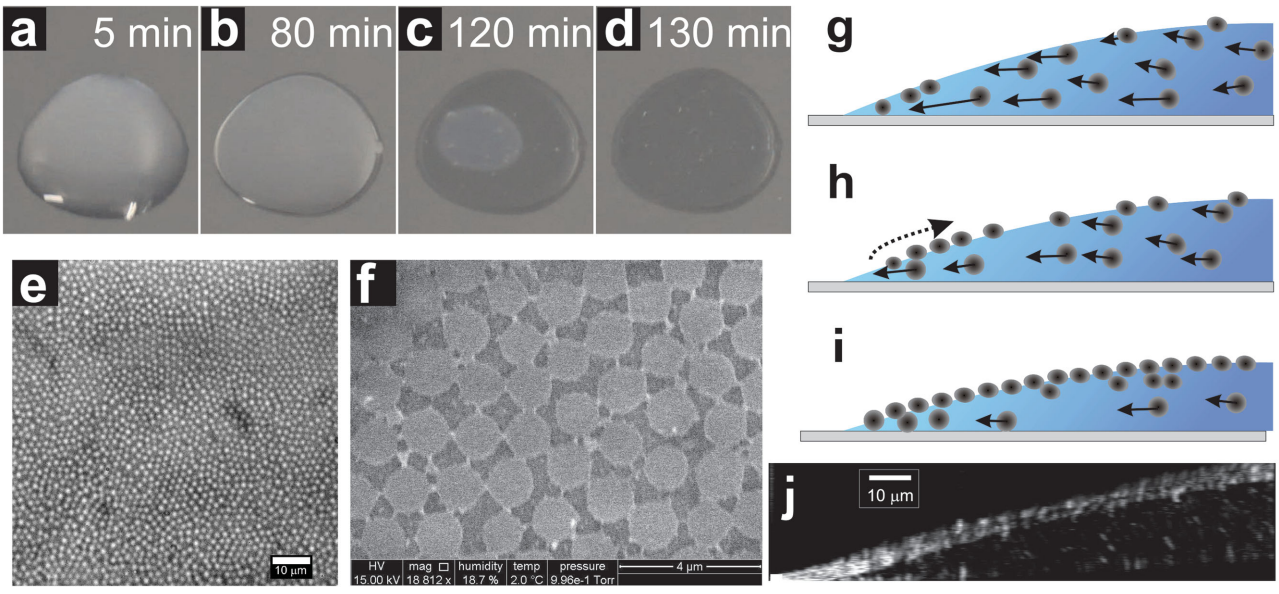

Figure 1. a–d) Photographs of drying water/PNIPAM/glutaraldehyde drop (V = 100 μL) on silicon wafer after approximately 15, 80, 120, and 130 min, respectively. Drop diameter is ≈1 cm. e) Micrograph of the center region of a membrane dried on a microscope cover slip (low ϕ). f) Environmental SEM picture of a dry cross–linked membrane on a silicon substrate before floating. g–i) Cartoons depicting the deposition process. g) Convective flows transport PNIPAM particles toward the three-phase contact line, and h,i) the particles often become attached to the air–water interface in the vicinity of the contact line. As the water evaporates, particles form a dense mono-layer. Excess PNIPAM particles can accumulate near the three-phase contact line, leading to a somewhat thicker membrane there [cf. (d)]. j) Confocal fluorescence micrograph averaged over 10 s of a drying drop of water containing fluorescently labeled PNIPAM particles on a cover slip. Particles populate the air–water interface.

to approximately 50 particle diameters. A micrograph of such a monolayer is shown in Figure 1e, in this case for a film grown on a microscope cover slip (with a contact angle of 30°–40°) at low ϕ. At relatively high experimental volume fractions, $\phi \approx 20\%–30\%$, the films are typically tens of particle layers thick. A drop with an area of 8 cm^2 made from 200 µL suspension ($\phi = 25\%$, $d = 2$ µm), for example, would produce a film of ≈40 particle layers in thickness (assuming uniform deposition). The formation of such layered structures arises because particles near the air–water interface are able to bind to the initial interfacial monolayer in situ due to the presence of cross-linker, i.e., while the drop is drying. In practice, we find that the films exhibit a coffee-ring-like structure with edges that are somewhat thicker than the center; these rims can be easily cut away with a razor blade while the film is still attached to the substrate.

In order to observe the films with higher resolution, environmental scanning electron microscopy (eSEM) was performed on the silicon substrate after film deposition. This technique permits SEM measurements in finite humidity and pressure, p.[32] In Figure 1f, a monolayer of PNIPAM particles can be clearly seen with neck-like connections between many neighboring particles, which we identify as interparticle cross-links. Note, under the eSEM conditions ($p \approx 100$ Pa, humidity < 20%), we expect the PNIPAM particles to be significantly smaller than when they are fully immersed in water.

The mechanism underlying the deposition process is depicted in Figure 1g–i. The pinned three-phase contact line drives the convective radial outward flow that transports PNIPAM particles toward the drop edge.[5] Instead of forming a coffee-ring-like structure, however, the PNIPAM particles near the drop edges attach to the air–water interface and many move radially toward the center of the drop.[17] We attribute the particles' tendency to attach to interfaces, in part, to the inherent amphiphilicity of the PNIPAM hydrogel particles, which stems from the chemical structure of PNIPAM and especially from the "loose" polymer chains that reside in the vicinity of the particle surface. In drops of linear PNIPAM chains dissolved in water, the polymer populates the air–water interface within seconds, as determined from surface tension measurements.[19,20] In microgel particle suspensions, PNIPAM particles require several minutes to populate the interface.[17,18] It is also known that the hydrogel particles flatten out partially when residing at water–air[18] or water–oil interfaces.[33–35] This effect also plays a role in their well-known ability to stabilize emulsions of the Pickering/"Mickering" type,[36] in which the deformed particles cover the oil–water interface more effectively than rigid spheres.[33]

Figure 1j shows a fluorescence confocal microscopy image of a drying water drop containing fluorescently labeled PNIPAM particles time-averaged over several seconds. The time-averaged image suggests that a relatively large concentration of PNIPAM particles populates the air–water interface (as schematically shown in Figure 1i, while other PNIPAM particles suspended in the bulk are transported toward the three-phase contact line. These observations, while limited, are consistent with explanations above and elsewhere.[37] Video S1 in the Supporting Information shows particles at the air–water interface in focus, along with particles flowing outward underneath the interfacial layer.

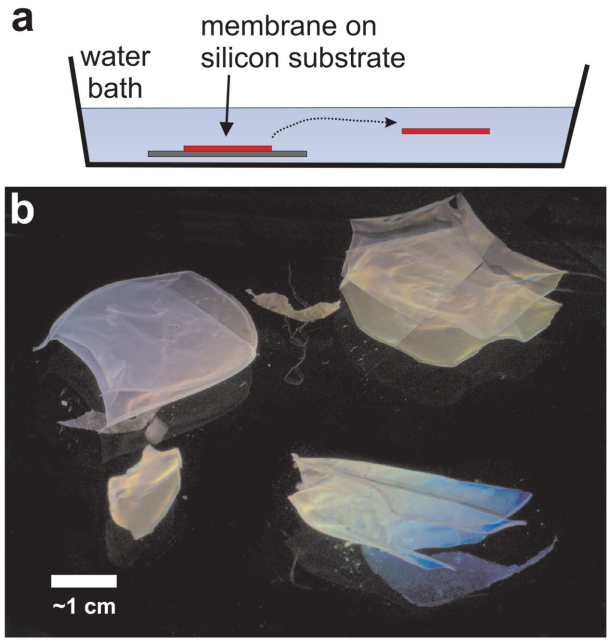

Figure 2. a) Cartoon depicting film–substrate water immersion and subsequent detachment and release of the film into the water. Films spontaneously detach from the silicon substrate in a water bath after approximately one day. b) PNIPAM films floating in a water bath with silicon substrate lying underneath (photographed from a side; colors come from thin film interference).

The deposition process depends on substrate properties. For example, on very hydrophilic glass substrates, the deposition process changes quite dramatically (cf. Video S2 in the Supporting Information). The contact line depins almost instantaneously, leading to a relatively uniform deposition. This latter effect is primarily found in samples with very high volume fractions of PNIPAM particles ($\phi \approx 30\%$). We speculate the depinning mechanism is similar to an effect found in evaporating droplets of water containing pluronic surfactant.[38,39] In short, the low contact angle of the glass substrate leads to thin droplets. Particles that are pushed toward the three-phase contact line are deposited several particle diameters inward of the contact line. The resultant particle layer apparently facilitates depinning of the contact line. We speculate that this effect is a result of further surface hydrophilization due to the deposited hydrogel particles. Unfortunately, the films grown on glass substrates that take advantage of this alternative deposition mechanism cannot be easily separated from their substrates. Therefore, we focused on experiments with silicon substrates.

After the film has formed on the substrate it is desirable to detach the film. We employ a simple strategy for deriving a freestanding film (**Figure 2**a). After 24 h of drying and cross-linking, we simply immerse the wafer with the film(s) into a bath of deionized water at room temperature. Over the course of 1–2 d, the hydrophilic films detach from the silicon substrate and then float in the water; a razor blade can also be used to remove the fully hydrated films. Note, it is much easier to handle films that are several particle diameters thick; monolayer particle films are susceptible to destruction even by gentle contact. Three exemplary films made from 200–300 µL

suspension droplets of suspension are shown in Figure 2b. These films float in water.

The resulting cm-size films are robust. When the films are folded and the suspension is gently stirred with a spatula, the films readily unfold without breaking. In addition, we did not observe any obvious signatures of film decomposition, e.g., due to insufficient cross–linking, over time-frames of several days to weeks.

The responsiveness of colloidal hydrogel films/membranes derives from the fact that many hydrogels are responsive to stimuli. In the case of PNIPAM and polymers of other aliphatic acrylamide derivatives, sensitivity is to temperature or pH. Furthermore, with introduction of responsive groups, chemosensitive molecular recognition is possible.[25] The films synthesized for this contribution utilize the inherent thermo-responsiveness of PNIPAM-particles to produce films/membranes with temperature-sensitive dimensions. Moreover, as PNIPAM particles respond to temperature variation, the particle elastic modulus changes with particle size following a power-law correlation;[40] this effect introduces mechanical softness as an additional parameter that can be tuned in our films.

In order to characterize these behaviors, we first measured the hydrodynamic diameter, d_H, of a source batch of PNIPAM particles as a function of temperature by dynamic light scattering. The variation in particle size (normalized by $d_{H,25\,°C} = 1.53$ µm, the diameter at 25 °C) is shown by the open diamonds in **Figure 3**. We next cut a small square-shaped colloidal monolayer film from a larger film; the square-shaped film is small enough to be observed using a 5× air objective via brightfield microscopy equipped with a temperature controlled heat stage (Mettler-Toledo). The heat stage permits investigation of the square-shaped film immersed in water as a function of temperature. Typically, the sample is heated from 25 °C to 35 °C, and then allowed to cool back to 25 °C. Exemplary pictures of the square-cut film are shown in the insets of Figure 3 at 25 °C (before and after the temperature cycle) and at 35 °C,

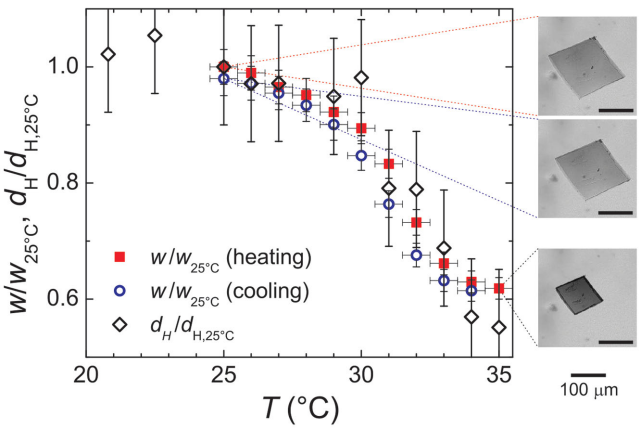

Figure 3. Dimensionless size $w/w_{25\,°C}$ of square-cut hydrogel film normalized by its size at 25 °C during heating (solid red squares) and cooling (open blue circles) between 25 and 35 °C in water. For comparison, the normalized hydrodynamic radius $d_H/d_{H,25\,°C}$ of the constituent particles is shown (open diamonds) in the same diagram ($d_{H,25\,°C} = 1.53$ µm). Pictures on the right show micrographs of the film at 25 °C (before and after heating cycle) and 35 °C, respectively.

respectively. We measure the length of the edges of the square at each temperature and thus extract the width of the film, w, again normalized by its value at 25 °C. The entire heating/cooling cycle is shown in Video S3 in the Supporting Information. The changes in film size as a function of temperature are reversible and clearly track variations in the diameter of the constituent hydrogel particles over this temperature range. This behavior confirms that neither cross-linking nor the deposition process significantly alter the individual particles' temperature sensitivity, which is fully imparted to the film. The lack of temperature hysteresis further corroborates our microscopic picture of this film of cross-linked hydrogel particles.

In the future it may be possible to employ these colloidal hydrogel films in membrane applications wherein tunable permeability is desired; the key for control of permeability, in this case, is their tunable pore size. In this context, it is useful to estimate pore size from the particle diameter d. For example, in a perfect close-packed 3D lattice of spheres, the smallest voids are the trigonal voids in each hexagonal layer. In order to fit through these voids, spherical particles must be smaller than $0.155d$. Thus, a lower limit for the pore size of our colloidal hydrogel films is about 15% of the particle diameter in the film; this pore size will, of course, change with temperature, making the films good candidates for the realization of functional membranes. If the films are randomly packed, a more realistic estimation of pore size can range up to $0.3d$. In future experiments, the exact pore size and pore distribution can be measured, e.g., using atomic force microscopy.

When we compare the gray scale of the brightfield microscopy images of the film at different temperatures, as shown in the insets of Figure 3 (cf. Video S3 in the Supporting Information), then we find that the film gets darker with increasing temperature. Thus optical transmission through the film varies reversibly with temperature. Superficially, the trends in transmitted intensity variation depends on average PNIPAM polymer density in the hydrogel; an increase in density will produce an increasing mismatch in the refractive index between polymer-rich regions and water/air.[41] The decrease in the intensity of transmitted light with increasing polymer density is in rough agreement with a simple Beer–Lambert approach treating the extinction coefficient of PNIPAM polymer as a free fit parameter. Importantly, scattering, rather than absorption, is the main contributor to the extinction coefficient, but modeling the change in light scattering as a function of temperature is nontrivial. However, as polymer density changes with temperature, both particle refractive index and particle size change.

To further investigate film optical properties, we perform another temperature-dependent transmission experiment over a broader temperature range (25–45 °C). The measurement employs an LED light source with a narrow bandwidth (FWHM ≈ 15 nm) and two different illumination wavelengths ($\lambda_1 = 660$ nm, $\lambda_2 = 470$ nm). In **Figure 4**a, we show the normalized intensity of the light transmitted through the film, $I_T/I_{25\,°C}$. At temperatures below ≈33 °C, I decreases monotonically with increasing temperature. Interestingly, however, at this temperature, I has a minimum and, with further temperature increments, I is observed to increase monotonically though much more slowly than it decreased at the lower temperatures. The

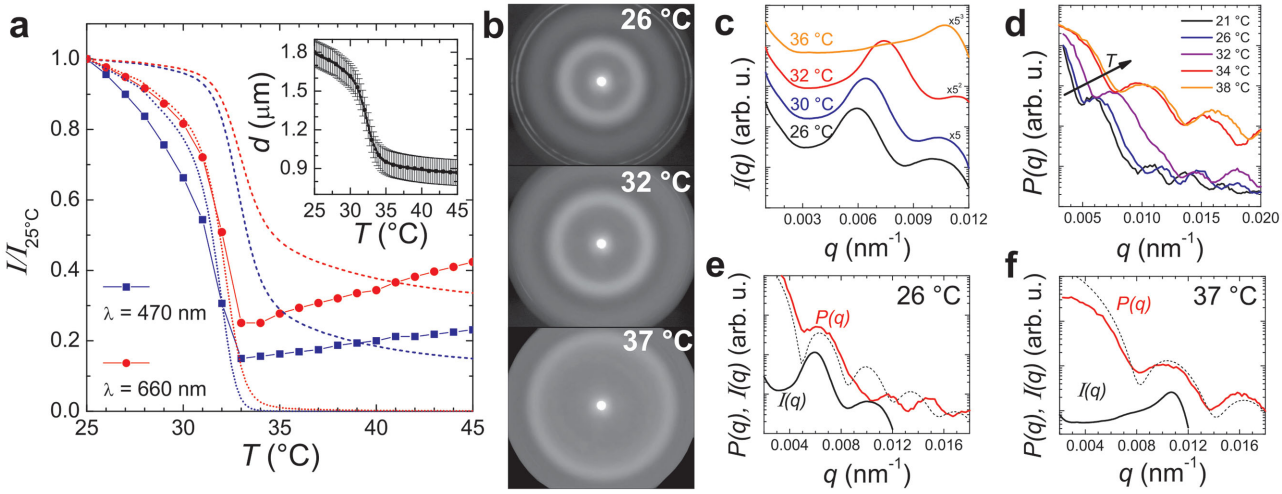

Figure 4. a) Transmittance $I(T)$ of the film normalized by the transmittance at 25 °C measured for $\lambda_1 = 660$ nm and $\lambda_2 = 470$ nm. The dashed lines are the expected curves based on an independent particle Mie scattering model for both wavelengths, assuming the film is eight layers thick; dotted lines assuming the film is fifty layers thick. Details and limitations of this simple model are discussed in the text. Inset: diameter d of PNIPAM particles in the film as a function of temperature, measured from the width of the film (with $d_{25\,°C} = 1.8$ μm [± 100 nm]); the solid line is an interpolation. b) Three exemplary optical measurements of $I(q)$ using an optical microscope with Bertrand lens. Images at three different temperatures are composed of four images with different integration times after conversion to a logarithmic intensity scale. c) $I(q)$ at different temperatures obtained from the Bertrand lens experiments by azimuthal averaging of the intensity of images in (b) (shifted for clarity). d) $P(q)$ at different temperatures obtained from static light scattering of a dilute aqueous suspension of the same particles that constitute the film. e,f) $I(q)$ from the microscope experiment in comparison to $P(q)$ measured by static light scattering from a dilute suspension of the constituent particles in water at two different temperatures. For comparison, the dashed line shows the theoretical Mie scattering of a single homogeneous sphere ($n_p = 1.34$; 1.40, $d = 1.81$; 1.07 μm, respectively, and 5% polydispersity).

curves are very similar for both wavelengths, but when illuminated at $\lambda_2 = 470$ nm, the transmittance dips about 10% deeper.

The film consists of several layers of PNIPAM particles that are cross-linked to each other (cf. Figure 1e); thus, it is tempting to treat the optical problem as the transmission of light through a slab of independent spherical scatterers. For optically homogeneous spherical particles with diameters similar to the wavelength of the probing light, i.e., $d \approx \lambda$, the individual scattering events can be described by Mie scattering theory.[42] The particle scattering cross section, σ_{sc}, depends on particle size relative to the wavelength of light, d/λ, and on the ratio between the refractive indices of the particles and the surrounding medium, n_p and n_s, respectively. We can qualitatively (and semiquantitatively) understand the changing transmission using the Mie scattering model. In particular, we assume that the spheres in the film are homogeneous with refractive index n_p that is directly proportional to the polymer density in the sphere (see the Supporting Information for details). Note, in this simple model we neglect multiple scattering and interference effects.

Using this model, the absorbance, $A = -\ln(I/I_0)$, depends on particle cross section σ_{sc}, particle number concentration, N, and light path length, l. The product of N and l is simply the number of particles per area encountered by the light beam. When we model the film as a stack of N_L monolayers, with an area packing fraction ϕ that is independent of temperature (because the film shrinks affinely), then we can express the light transmission simply in terms of the scattering efficiency $Q_{sc} = 4\sigma_{sc}/(\pi d^2)$. Thus, the transmittance becomes

$$I/I_0 = \exp(-A) = \exp(-\sigma_{sc} N l) = \exp(-Q_{sc}\phi N_L) \quad (1)$$

We use a published IDL algorithm[43] to calculate Q_{sc} as a function of temperature, and we assume $\phi \approx 0.8$ near random close packing in two dimensions. Moreover, we can correct for the direction in which the light is scattered and detected, which depends on the numerical aperture of our objective; this is a minor correction discussed in the Supporting Information.

In Figure 4a, we show the calculated transmittance normalized by its value at 25 °C. For modeling this film, we varied the number of layers, N_L. We found that the overall decrease in transmittance is captured by a range of layer thicknesses from $N_L \approx 8$ to $N_L \approx 50$. Note, the eight layer curve best captures the change in intensity between temperature extrema, but the fifty layer curve best captures the shape of the intensity curve for temperatures below 33 °C. Moreover, the total transmittance at 25 °C, $I_{25\,°C}/I_0$, is captured fairly well using $N_L = 50$ with $I_{25\,°C}/I_0 \approx 0.7$; by contrast, $I_{25\,°C}/I_0 \approx 0.95$ for $N_L = 8$ (see the Supporting Information).

Direct comparison of theoretical and experimental curves suggests that our simple model exhibits the general trends observed in the optical transmission experiment. Overall, however, the agreement is mediocre. For $N_L = 8$, the slopes, dI/dT, are different over almost the entire temperature range, and the rise in transmittance at temperatures above 33 °C is not reproduced. For $N_L = 50$, on the other hand, the model exhibits significant deviations from the experimental data at $T > 33$ °C, where the calculated curve decreases asymptotically to zero. Furthermore, variation of n_p or N_L changes the result only gradually and does not alter the general shape of the curves (see the Supporting Information). These differences between theory and experiment, however, are not too surprising because the model makes some fairly severe approximations. For example,

it is known that PNIPAM microgels are nonuniformly cross-linked (when synthesized following the one-pot scheme[44] and, to a lesser extent, the semibatch scheme[13]; a higher cross-linking and polymer density occurs in the center of the particles, which leads to a heterogeneous n_p within each particle. Also, recall that we have neglected interference and multiple scattering effects that arise between particles, an oversimplification for such dense particle packings.

According to Bohren and Huffman,[42] multiple scattering can safely be neglected as long as absorbance is low, i.e., $A << 1$. In our experiments, $A \approx 0.3$ for the lowest temperatures, but is >1 at the higher temperatures; it monotonically increases with temperature as a result of the increasing mismatch between n_p and n_s. Therefore, we conclude that the most likely explanation for the peculiar behavior at high temperatures is a result of increasingly important multiple scattering effects with increasing temperature.

To obtain further insights into the film's optical transmission, we performed two additional light scattering experiments whose results are given in Figure 4b–f. First, we directly measured the scattering of light in transmission with a narrow bandwidth spectral filter (i.e., an interference bandpass filter with FWHM ≈ 10 nm at $\lambda = 650$ nm) by inserting a Bertrand lens into the optical path of a light microscope. We employed a CCD camera to record the diffraction patterns as a function of temperature (Figure 4b). The absence of a point scattering pattern indicates the absence of long-range crystalline order. (Accordingly, the pore size distribution in the membrane is probably spatially heterogeneous.)

In Figure 4c, we show the scattered intensity, $I(q)$, at different temperatures; it is obtained by azimuthal averaging of the scattering intensity multiplied by $\sin(\theta)$ and corrected for the solid angle of each pixel. The scattering angle, θ, is related to the scattering wave vector, q, by $q = 4\pi n_s/\lambda \sin(\theta/2)$. (For details of the angle and temperature calibration, see the Supporting Information.) The most striking features of these spectra are the position and intensity of the first peak, which shifts to higher q and becomes less pronounced with increasing temperature, i.e., with decreasing particle diameter.

Next, we compare $I(q)$ to the particle form factor $P(q)$. To this end, we measure static light scattering of a dilute sample of the uncross-linked PNIPAM particles in water at different temperatures (Figure 4d); we utilize a Brookhaven Instruments BI-200SM setup equipped with a 100 mW Nd:YAG-laser ($\lambda = 532$ nm) for the measurements. In Figure 4e,f, a direct comparison of $I(q)$ and $P(q)$ is given at a low and a high temperature, respectively. Interestingly, at both temperatures, the position of the first peak is the same in both experiments, i.e., it seems that single particle scattering dominates the directional scattering at angles $\theta >> 0°$ of the films. On the other hand, both experiments clearly deviate at low q. The scattering intensity increases much more strongly for $q \to 0$ in the dilute sample than in the film experiment. This finding can be readily rationalized due to a nonnegligible film structure factor $S(q) = I(q)/P(q)$. In a dense 2D packing, $S(q) < 1$ for $q < 2\pi/d$, thus the forward scattering of the films is reduced compared to the static light scattering experiment. Accordingly, these observations confirm the limitations of the simple model used in Figure 4a. In a similar vein, $P(q)$ deviates significantly from the theoretical curves (dashed) calculated using Mie scattering; the deviation is largest for the low temperatures wherein PNIPAM particles are known to be nonhomogeneous in density. Thus, we can conclude that the transmission of light through our colloidal films is influenced by both interference and multiple scattering effects which help explain deviations between our simple model and experiment. A detailed model of this very complex scattering problem, however, is beyond the scope of the present paper.

3. Conclusion

In summary, we introduced a methodology to prepare thin colloidal hydrogel films/membranes simply by evaporating sessile suspension droplets. Films constructed via this method range in thickness from a few particle diameters to tens of particle diameters, and they retain their constituent particles' temperature responsiveness, i.e., they shrink and expand with increasing and decreasing temperature, respectively. This behavior could prove useful, because membranes with adjustable porosity can be employed to realize switchable filters or to build thermo-mechanical attenuators.[45,46] Additional functionalities could also be introduced into these systems. Some potentially useful platforms for the cross-linked colloidal hydrogel-particle films include structures of various shapes (e.g., similar to hydrogel colloidosomes),[47,48] bilayer formation for self-folding "origami" structures,[49,50] and handling of cultured cells.[51,52]

Furthermore, we demonstrated and rationalized interesting optical transmission properties which also vary with temperature; these properties stem from the scattering of constituent particles. In principle, optical transmission through these films can also be used to sense local environment. For specific technical applications, it will be important to explore additional preparation techniques. For example, dip coating or doctor blading methods could prove useful and will be explored in future studies.

Supporting Information

Supporting Information is available from the Wiley Online Library or from the author.

Acknowledgements

The authors thank P. Collings, R. Composto, R. Dreyfus, Z. Fakhraai, M. Gratale, and D. Lee for helpful discussions and J. Ford for help with the eSEM measurement. The authors gratefully acknowledge financial support from the National Science Foundation through Grant Nos. PENN MRSEC DMR11-20901 and DMR12-05463 and through MRSEC shared experimental facilities for optical and electron microscopy; the authors also acknowledge partial support from NASA Grant No. NNX08AO0G. K.H. acknowledges funding through the Penn REU program.

Received: July 10, 2015
Published online: August 21, 2015

[1] T. Peng, Y.-L. Cheng, *J. Appl. Polym. Sci.* **1998**, *70*, 2133.
[2] L.-Y. Chu, Y. Li, J.-H. Zhu, H.-D. Wang, Y.-J. Liang, *J. Control. Release* **2004**, *97*, 43.

[3] L.-Y. Chu, Y. Li, J.-H. Zhu, W.-M. Chen, *Angew. Chem. Int. Ed.* **2005**, *44*, 2124.
[4] L. Chu, R. Xie, X. Ju, *Chin. J. Chem. Eng.* **2011**, *19*, 891.
[5] R. D. Deegan, O. Bakajin, T. F. Dupont, G. Huber, S. R. Nagel, T. A. Witten, *Nature* **1997**, *389*, 827.
[6] N. D. Denkov, O. D. Velev, P. A. Kralchevsky, I. B. Ivanov, H. Yoshimura, K. Nagayama, *Nature* **1993**, *361*, 26.
[7] H. Hu, R. G. Larson, *J. Phys. Chem. B* **2002**, *106*, 1334.
[8] B. M. Weon, J. H. Je, *Phys. Rev. E* **2010**, *82*, 015305.
[9] P. J. Yunker, T. Still, M. A. Lohr, A. G. Yodh, *Nature* **2011**, *476*, 308.
[10] H. B. Eral, D. M. Augustine, M. H. G. Duits, F. Mugele, *Soft Matter* **2011**, *7*, 4954.
[11] A. P. Sommer, N. Rozlosnik, *Cryst. Growth Des.* **2005**, *5*, 551.
[12] T. Kajiya, W. Kobayashi, T. Okuzono, M. Doi, *J. Phys. Chem. B* **2009**, *113*, 15460.
[13] T. Still, P. J. Yunker, A. G. Yodh, *Langmuir* **2012**, *28*, 4984.
[14] L. Cui, J. Zhang, X. Zhang, Y. Li, Z. Wang, H. Gao, T. Wang, S. Zhu, H. Yu, B. Yang, *Soft Matter* **2012**, *8*, 10448.
[15] A. Crivoi, F. Duan, *Langmuir* **2013**, *29*, 12067.
[16] A. Crivoi, F. Duan, *Phys. Rev. E* **2013**, *87*, 042303.
[17] K. Horigome, D. Suzuki, *Langmuir* **2012**, *28*, 12962.
[18] J. Zhang, R. Pelton, *Langmuir* **1999**, *15*, 8032.
[19] J. Zhang, R. Pelton, *Langmuir* **1996**, *12*, 2611.
[20] J. Zhang, R. Pelton, *Colloids Surf., A* **1999**, *156*, 111.
[21] R. Pelton, *Adv. Colloid Interf. Sci.* **2000**, *85*, 1.
[22] I. Tokarev, V. Gopishetty, J. Zhou, M. Pita, M. Motornov, E. Katz, S. Minko, *ACS Appl. Mater. Interfaces* **2009**, *1*, 532.
[23] I. Tokarev, S. Minko, *Adv. Mater.* **2010**, *22*, 3446.
[24] E. Mah, R. Ghosh, *Processes* **2013**, *1*, 238.
[25] J. H. Holtz, S. A. Asher, *Nature* **1997**, *389*, 829.
[26] L.-Y. Chu, T. Niitsuma, T. Yamaguchi, S.-I. Nakao, *AIChE J.* **2003**, *49*, 896.
[27] F. Yan, W. Goedel, *Adv. Mater.* **2004**, *16*, 911.
[28] S. Reculusa, B. Agricole, A. Derr, M. Couzi, E. Sellier, S. Ravaine, P. Delhas, *Adv. Mater.* **2006**, *18*, 1705.
[29] T. Still, K. Chen, A. M. Alsayed, K. B. Aptowicz, A. Yodh, *J. Coll. Int. Sci.* **2013**, *405*, 96.
[30] A. M. Alsayed, Y. Han, A. Yodh, *Microgel Suspensions* (Eds: A. Fernandez-Nieves, H. M. Wyss, J. Mattsson, D. A. Weitz), Wiley-VCH, Weinheim, Germany **2011**, pp. 229–281.
[31] R. D. Deegan, *Phys. Rev. E* **2000**, *61*, 475.
[32] M. J. Garcia-Salinas, A. M. Donald, *J. Colloid Interface Sci.* **2010**, *342*, 629.
[33] W. Richtering, *Langmuir* **2012**, *28*, 17218.
[34] K. Geisel, L. Isa, W. Richtering, *Langmuir* **2012**, *28*, 15770.
[35] K. Geisel, W. Richtering, L. Isa, *Soft Matter* **2014**, *10*, 7968.
[36] S. Schmidt, T. Liu, S. Rutten, K.-H. Phan, M. Moller, W. Richtering, *Langmuir* **2011**, *27*, 9801.
[37] N. Vogel, C. Fernndez-Lpez, J. Prez-Juste, L. M. Liz-Marzn, K. Landfester, C. K. Weiss, *Langmuir* **2012**, *28*, 8985.
[38] L. Cui, J. Zhang, X. Zhang, L. Huang, Z. Wang, Y. Li, H. Gao, S. Zhu, T. Wang, B. Yang, *ACS Appl. Mater. Interfaces* **2012**, *4*, 2775.
[39] P. Yunker, A. G. Yodh, T. Still, *Proc.Int. School of Physics "Enrico Fermi" Course CLXXXIV Physics of Complex Colloids* (Eds: C. Bechinger, F. Sciortino, P. Ziherl), IOS, Amsterdam, Netherlands **2013**.
[40] K. N. Nordstrom, E. Verneuil, W. G. Ellenbroek, T. C. Lubensky, J. P. Gollub, D. J. Durian, *Phys. Rev. E* **2010**, *82*, 041403.
[41] B. W. Garner, T. Cai, S. Ghosh, Z. Hu, A. Neogi, *Appl. Phys. Express* **2009**, *2*, 057001.
[42] C. F. Bohren, D. R. Huffman, *Absorption and Scattering of Light by Small Particles*, John Wiley & Sons, Inc., Weinheim **1998**.
[43] Mie scattering code, University of Oxford, http://www.atm.ox.ac.uk/code/mie/, accessed: May 2014.
[44] M. Stieger, W. Richtering, J. S. Pedersen, P. Lindner, *J. Chem. Phys.* **2004**, *120*, 6197.
[45] K. K. Westbrook, H. J. Qi, *J. Intel. Mat. Syst. Str.* **2008**, *19*, 597.
[46] R. Fuhrer, E. K. Athanassiou, N. A. Luechinger, W. J. Stark, *Small* **2009**, *5*, 383.
[47] R. K. Shah, J.-W. Kim, D. A. Weitz, *Langmuir* **2010**, *26*, 1561.
[48] W. Wang, A. H. Milani, L. Carney, J. Yan, Z. Cui, S. Thaiboonrod, B. R. Saunders, *Chem. Commun.* **2015**, *51*, 3854.
[49] T. S. Shim, S.-H. Kim, C.-J. Heo, H. C. Jeon, S.-M. Yang, *Angew. Chem. Int. Ed.* **2012**, *51*, 1420.
[50] J.-H. Na, A. A. Evans, J. Bae, M. C. Chiappelli, C. D. Santangelo, R. J. Lang, T. C. Hull, R. C. Hayward, *Adv. Mater.* **2015**, *27*, 79.
[51] S. Schmidt, M. Zeiser, T. Hellweg, C. Duschl, A. Fery, H. Möhwald, *Adv. Funct. Mater.* **2010**, *20*, 3235.
[52] D. Chen, R. D. Hyldahl, R. C. Hayward, *Lab Chip* **2015**, *15*, 1160.

